Lung Cancer 147 (2020) 56–63

Contents lists available at ScienceDirect

Lung Cancer

journal homepage: www.elsevier.com/locate/lungcan

Gene expression profiling by targeted RNA sequencing in pathological stage I lung adenocarcinoma with a solid component

Yoshiteru Kidokoro[a,b,1], Tomohiko Sakabe[a,1], Tomohiro Haruki[b], Taichi Kadonaga[a,b], Kanae Nosaka[a], Hiroshige Nakamura[b], Yoshihisa Umekita[a,*]

[a] Division of Pathology, Department of Pathology, Department of Surgery, Faculty of Medicine, Tottori University, Tottori, Japan
[b] Division of General Thoracic Surgery, Department of Surgery, Faculty of Medicine, Tottori University, Tottori, Japan

ARTICLE INFO

Keywords:
Solid component
Lung adenocarcinoma
Differentially expressed gene

ABSTRACT

Objectives: Solid predominant adenocarcinoma is considered an independent predictor of an unfavorable prognosis in patients with stage I lung adenocarcinoma (LUAD). Furthermore, solid minor components are related to poor prognosis in patients with stage I LUAD. Therefore, it is imperative to elucidate the molecular determinants of the malignant potential of solid components (SC). Several studies reported the gene expression profiling specific for lepidic predominant adenocarcinoma or solid predominant adenocarcinoma, however; there is no report identifying the differentially expressed genes (DEGs) between SC and acinar component (AC) within the same tumor tissue in pathological (p)-stage I LUAD patients.

Materials and Methods: LUAD tissue samples containing both SC and AC were obtained from 8 patients with p-stage I LUAD and each component was microdissected. Targeted RNA sequencing was performed by a high-throughput chip-based approach.

Results: In total, 1272 DEGs were identified, including 677 upregulated genes and 595 downregulated genes in SC compared with AC. The most highly upregulated gene was TATA binding protein associated factor 7 (*TAF7*) and the most highly downregulated gene was homeobox B3 (*HOXB3*), which acts as a metastasis suppressor. A protein–protein interaction (PPI) network analysis of upregulated genes in SC identified ribosomal protein S27a (*RPS27a*) as a hub gene with the highest degree. First neighbors of RPS27a included PSMA6, which is a highly promising target for lung cancer. The subnetwork of PD-L1 had 10 first neighbors, including CMTM6, which enhances the ability of PD-L1-expressing tumor cells to inhibit T cells. The staining score for PD-L1 in SC was significantly higher than that in AC by immunohistochemistry ($p = 0.001$).

Conclusion: Our results revealed several new DEGs and key PPI network in SC compared to AC, contributing to understanding the biological features of SC and providing therapeutic targets for early-stage LUAD with SC in the future.

1. Introduction

Adenocarcinoma is the most common histological type of lung cancer in most countries, accounting for almost half of all lung cancer cases [1]. Invasive adenocarcinoma shows heterogeneous morphological features and is classified into lepidic, acinar, papillary, micropapillary, and solid subtypes based on the predominant histological pattern [1].

Although surgical resection improves the long-term survival of patients with early-stage lung cancer, the 5-year survival rates for pathological (p)-stage IA1, IA2, IA3 and IB are 90 %, 85 %, 80 %, and 73 %, respectively, according to the eighth edition of the Tumor, Node and Metastasis (TNM) Classification for lung cancer [2]. The histological heterogeneity is considered to be a main contributor to differences in clinical outcomes among patients with stage I lung adenocarcinoma (LUAD). For example, several studies have shown that clinical outcomes are unfavorable for solid predominant adenocarcinoma (SPA) and/or micropapillary predominant adenocarcinoma in patients with stage I LUAD [3–7]. We and others have reported that LUAD with a solid component (SC) shows poor prognosis, even if the SC is not predominant [8–10]. However, the biological features of SC leading to unfavorable prognosis are largely unknown. Rekhtman N, *et al.*

* Corresponding author at: Division of Pathology, Department of Pathology, Faculty of Medicine, Tottori University, 86 Nishicho, Yonago, Tottori 683-8503, Japan.
E-mail address: yume@tottori-u.ac.jp (Y. Umekita).
[1] These authors contributed equally to this work.

https://doi.org/10.1016/j.lungcan.2020.06.035
Received 2 December 2019; Received in revised form 15 May 2020; Accepted 29 June 2020

reported that solid pattern was over-represented in LUAD with KRAS mutation [11]. On the other hand, Hu H, et al. reported that solid pattern exhibited a significantly higher pan-negative mutation frequency and a lower EGFR mutation frequency compared with non-solid pattern [12], suggesting that the association between SC and driver mutations remains controversial. This prompted us to investigate the biological and molecular features of SC in patients with LUAD. Several recent studies have reported the specific gene expression profiles for lepidic predominant adenocarcinoma [13] or SPA [14–17]. However, to our knowledge, differentially expressed genes (DEGs) between the SC and acinar component (AC), which is also known as the most popular component among the histologic subtype of LUAD [3,9], within the same tumor tissue in patients with p-stage I LUAD have not been identified. The comparison between SC and AC within the same tumor tissue by targeted RNA sequencing [18] may be helpful for the identification of specific genes responsible for the malignant potential of SC. These specific genes could contribute to understanding the biological features of SC and the development of therapeutic applications in the future. We performed the first gene expression profiling analysis of different components within the same tumor tissues in patients with p-stage I LUAD.

2. Materials and methods

2.1. Patient selection and histological evaluation

A total of 255 consecutive patients who underwent curative surgical resection for LUAD diagnosed as p-stage IA1–IB according to the eighth edition of TNM Classification from January 2014 to December 2017 were recruited. Among these patients, eight surgical specimens were selected according to the following two criteria: (1) SPA with an acinar component of > 10 % and (2) acinar predominant adenocarcinoma with a solid component of > 10 %. Additionally, the area of cribriform pattern in acinar component was evaluated. Supplementary Table 1 summarizes the patient's backgrounds. The following specimens were excluded: SPA with mucin, invasive adenocarcinoma with signet-ring cell features or with a micropapillary component of > 1 %, and special types of invasive adenocarcinoma, like colloid adenocarcinoma. Patients who underwent neo-adjuvant treatment were also excluded. Written informed consent for the use of data was obtained from all patients, and the study was approved by the Tottori University Ethical Review Board Japan (approval number: 17A124, March 8, 2018).

2.2. Sample preparation and RNA isolation

Surgically resected LUAD tissue was fixed in 10 % neutral buffered formalin for 24–48 h and embedded in paraffin. Then, 10 μm-thick sections were cut from paraffin blocks and attached to RNase-free certified polyethylene naphthalate membrane glass slides (Leica Microsystems, Wetzlar, Germany). These sections were deparaffinized and stained with Paradise Plus Stain (ARCTURUS Paradise PLUS FFPE LCM Staining Kit; Thermo Fisher Scientific, Waltham, MA, USA). SC and AC were separately microdissected using the LMD7000 (Leica Microsystems) and collected into 0.5 mL plastic tubes. Fig. 1 shows representative images of SC and AC stained with hematoxylin and eosin (Fig. 1A) or Paradise Plus Stain after laser capture microdissection (Fig. 1B). Finally, total RNA was extracted from the microdissected tissue using the Recover All Total Nucleic Acid Isolation Kit for FFPE (Thermo Fisher Scientific) according to the manufacturer's instructions. For RNA quality assessment, the DV_{200} value was calculated using the Agilent 2100 Bioanalyzer system according to the manufacturer's instructions (Agilent Technologies, Santa Clara, CA, USA). Sample #5 exhibited RNA fragmentation and was excluded from the analysis. Finally, 14 samples were analyzed by next-generation sequencing.

2.3. Targeted RNA sequencing

According to the manufacturer's instruction, gene expression was evaluated using an Ion Ampliseq™ Transcriptome Human Gene Expression Kit (Thermo Fischer Scientific). Complementary DNA (cDNA) was obtained from the reverse transcription of 100 ng of total RNA using a SuperScript™ VILO™ cDNA Synthesis Kit (Thermo Fischer Scientific). Libraries were prepared using an Ion AmpliSeq™ Library Kit Plus (Thermo Fischer Scientific) following by the amplification of targets using an Ion AmpliSeq™ Transcriptome Human Gene Expression Panel (Thermo Fischer Scientific). Finally, libraries were loaded and sequenced on the Ion Proton™ system using IonXpress™ Chip Type P1.1.17 (Thermo Fischer Scientific).

2.4. Statistical analyses

Ion Proton Torrent Suit v5.0.5 (Thermo Fischer Scientific) was used to map reads to the human genome hg19 as a reference genome. Using R v.3.51 (https://www.r-project.org), reads in raw sequence data files were counted using featureCounts (http://bioconductor.org). Samples with fewer than 1,000,000 reads were excluded and thus sample #6 was not suitable for analysis. Read counts for genes in six SC and six AC samples were compared using pairwise likelihood ratio tests to identify DEGs. False discovery rate (FDR) < 0.05 was used to estimate significance. Log_2 (fold change) > 0 was set as the threshold to identify upregulated genes in SC and log_2 (fold change) < 0 was used to identify downregulated genes in SC. A gene ontology (GO) enrichment analysis was performed to evaluate gene functions using the Database for Annotation, Visualization, and Integrated Discovery (DAVID) Bioinformatics Resources 6.8 (https://david.ncifcrf.gov) and the GO enrichment data were transferred to Reduce Visualize Gene Ontology (REVIGO; http://revigo.irb.hr) for visualization [19]. Kyoto Encyclopedia Genes and Genomes (KEGG) pathway analyses were also performed using DAVID. The protein–protein interaction (PPI) network for all upregulated genes in SC was evaluated using the Search Tool for the Retrieval of Interacting Genes/Proteins (STRING) v.10.5 [20]. Based on the PPI information from the STRING database, the PPI network of upregulated genes in SC was constructed using Cytoscape [21].

2.5. Immunohistochemical staining and evaluation

A total of 41 LUAD samples containing both AC (≥10 %) and SC (≥10 %) were resected. After the sections (4 μm thick) were deparaffinized and endogenous peroxidase activity was blocked, they were pretreated in EDTA buffer (1 mM, pH 8.0) at 100 °C for 15 min (for PD-L1), in citrate buffer (10 mM, pH 6.0) at 100 °C for 5 min (for TAF7), or in citrate buffer (10 mM, pH 6.0) at 100 °C for 10 min (for HOXB3). After cooling to room temperature, nonspecific binding was blocked by blocking buffer (BLOCK ACE; Megmilk Snow Brand, Sapporo, Japan). The sections were incubated at 4 °C overnight with an antibody for PD-L1 (E1L3N, diluted 1:400; Cell Signaling Technology, Inc., Danvers, MA, USA) [8], TAF7 (HPA006429, diluted 1: 500; Atlas Antibodies, Stockholm, Sweden), or HOXB3 (ab83404, diluted 1:500; Abcam, Inc., Cambridge, UK). Samples were then incubated with EnVision + System HRP (DAKO, Glostrup, Denmark) or VECTASTAIN Universal Elite ABC Kit (Vector Laboratories, Inc., Burlingame, CA, USA) according to the manufacture's protocol. Finally, the slides were incubated with diaminobenzidine (DAB) solution (liquid DAB + substrate, imidazole − HCl buffer, pH 7.5, containing hydrogen peroxide and anti-microbial agent; DAKO) for 5 min (for PD-L1), 4 min (for TAF7), or 1 min (for HOXB3). When cancer membranes for SC or AC were stained with a PD-L1 antibody, regardless of the staining intensity, the cases were considered PD-L1-positive. Samples were further divided into four categories according to the ratio of PD-L1 expression as follows: ≥50 % (score 3), 10–49 % (score 2), 1–9 % (score 1), and < 1 % (score 0). When the nuclei of SC or AC were stained with TAF7 antibody, the cases were

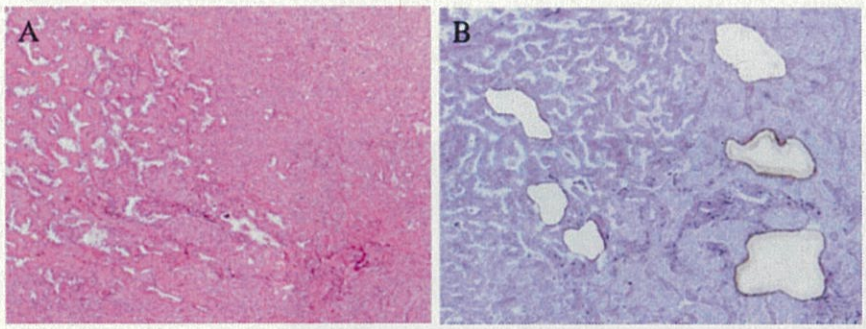

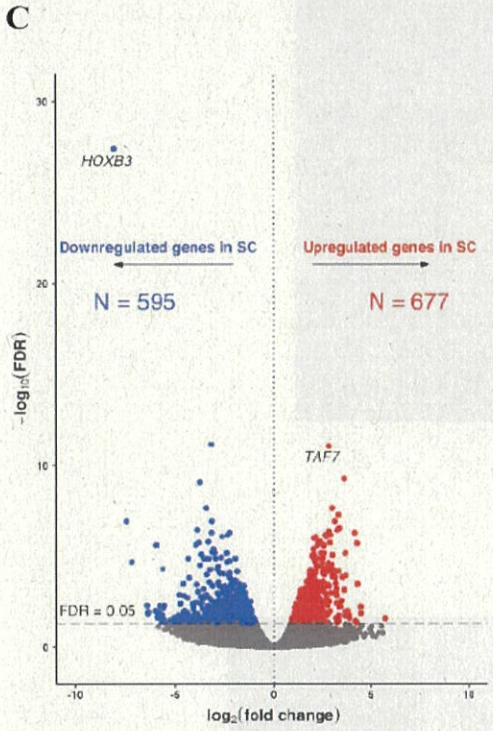

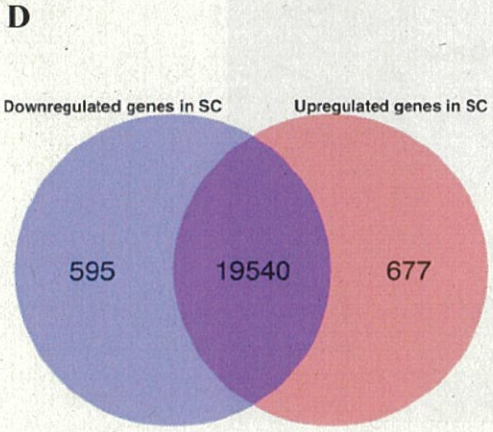

Fig. 1. A) Histology of the solid component (right half) and acinar component (left half) in sample 2 (hematoxylin & eosin stain).
B) Histology after laser capture microdissection (Paradise Plus Stain).
C) Volcano plot showing the pairwise comparison between solid component (SC) and acinar component (AC) of lung adenocarcinoma. The horizontal dotted line represents a false discovery rate (FDR) of 0.05 and FDR < 0.05 was used as the threshold for the identification of differentially expressed genes (DEGs). Red dots highlight genes that are upregulated in SC. Blue dots highlight genes that are downregulated in SC.
D) Venn diagram showing the shared profile of the upregulated and downregulated genes in SC.

considered TAF7-positive. TAF7 staining was quantified by following two metrics: the immunostaining-positive area (score 3; ≥50 %, score 2; 10–49 %, score 1; 1–9 %, score 0; < 1 %), and the staining intensity (score 3; 3+, score 2; 2+, score 1; 1+, score 0; 0). Staining scores of TAF7 were then calculated by multiplying these two metrics. When the nucleoli of SC or AC with more than 10 % were stained with HOXB3 antibody, regardless of the staining intensity, the samples were considered HOXB3-positive. All slides were evaluated by two pathologists

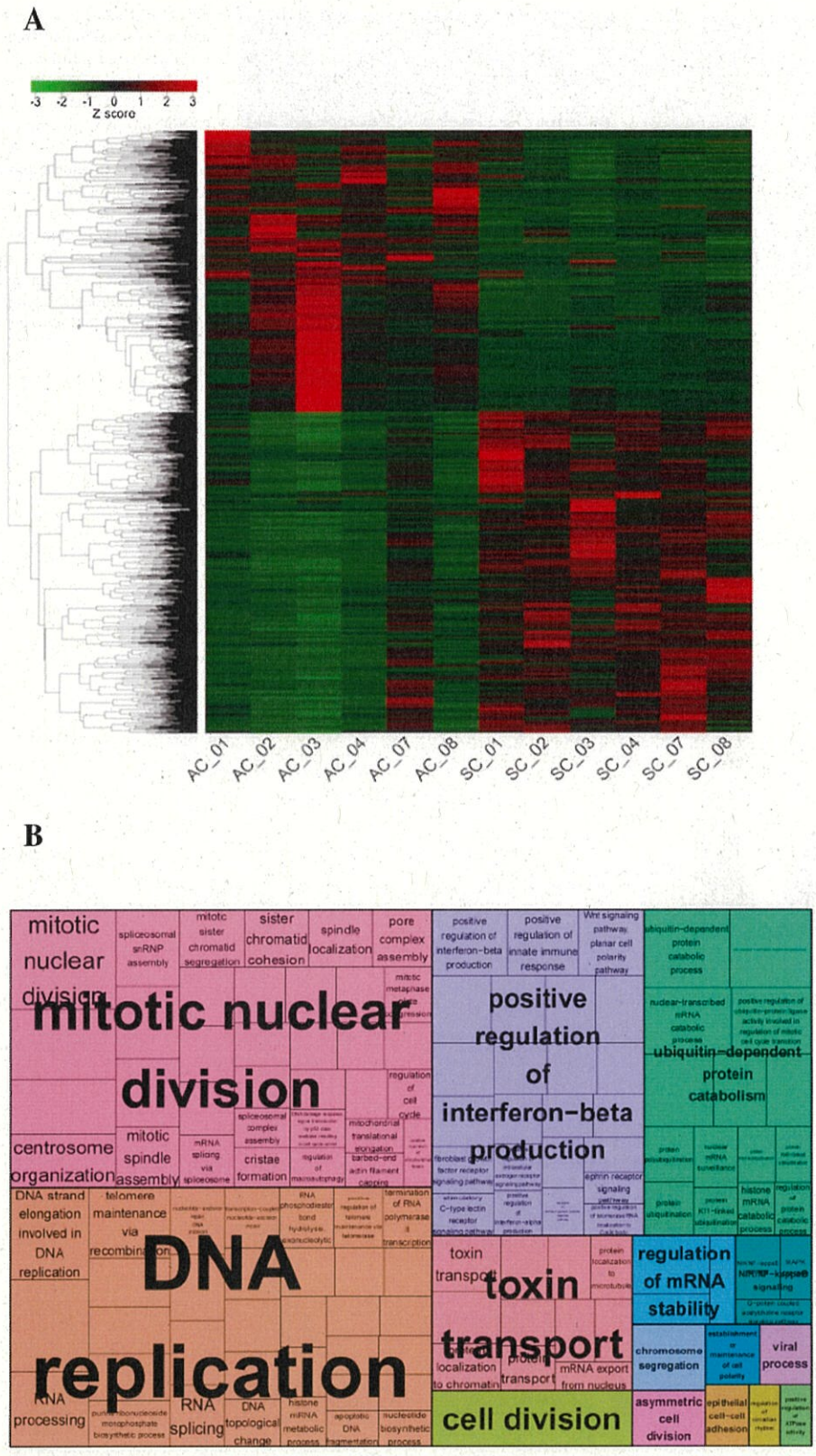

Fig. 2. A) Heat map showing differentially expressed genes in the solid component (SC) and acinar component (AC).
B) A TreeMap summarizing enriched gene ontology (GO) terms for upregulated genes in the solid component. The size of the small square in the large segment is proportionate to the number of GO terms.

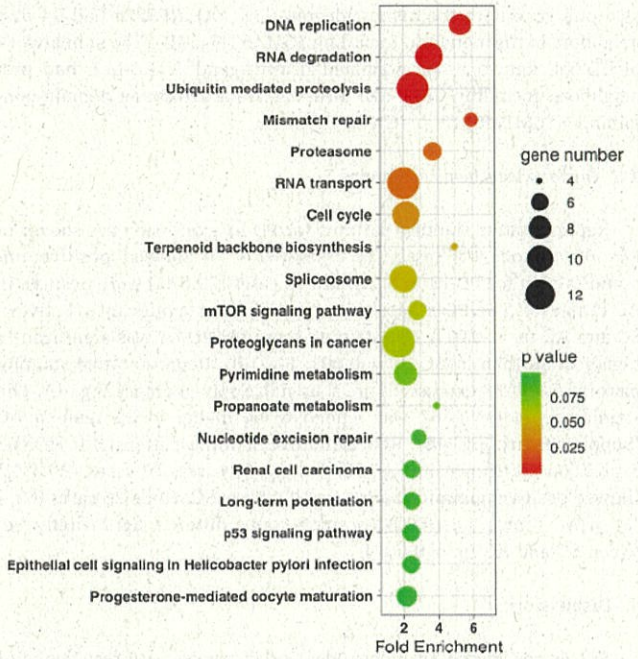

Fig. 3. Kyoto Encyclopedia of Genes and Genomes (KEGG) pathway enrichment analysis. *X*-axis represents the fold enrichment value and *Y*-axis represents the KEGG annotation cluster.

(Y.K. and Y.U.) and a final agreement was reached by discussion when the initial evaluations differed. Positive and negative scores were compared using the χ^2 test and the scores for SC and AC were compared using the Mann–Whitney *U* test Statistical significance was defined as $p < 0.05$.

3. Results

3.1. Transcriptome sequencing and gene expression analyses

Two RNA-sequencing runs were performed for each set of samples (1 set; 7 samples). In total, 12 million reads per sample were obtained with a mean read length of 95 bp and, a Q20 corresponding to a predicted error rate of 1 % was 91.87 % (Supplementary Table 2). After sequencing, sample #6 was not suitable for further analysis owing to the poor quality and low quantity of RNA (Supplementary Fig. 1). Thus, 20,813 genes were obtained from the raw sequence data mapped to the human reference genome hg19. A good performance of normalization using egdeR was achieved for 12 samples (Supplementary Fig. 2). In total, 1272 DEGs were identified (FDR < 0.05), including 677 upregulated genes in SC and 595 downregulated genes in SC (Fig. 1C, 1D and Supplementary Fig. 2,3). The most highly upregulated gene in SC was TATA binding protein associated factor 7 (*TAF7*) and the most highly downregulated gene in SC was homeobox B3 (*HOXB3*). A heatmap of DEGs showed a clear distinction between SC and AC (Fig. 2A).

3.2. Enrichment analysis and protein–protein interaction network

In total, 137 GO terms in the biological process category were enriched in the upregulated genes in SC using the Annotation cluster tool of the DAVID web server. REVIGO was used to summarize and visualize the GO terms. Fifteen clusters with related functions were identified and are represented by a TreeMap in Fig. 2B. In particular, the majority of GO terms were associated with cell proliferation, including "mitotic nuclear division" (35 GO terms) and "DNA replication" (34 GO terms) (Supplementary Table 3, 4). In the KEGG pathway enrichment analysis

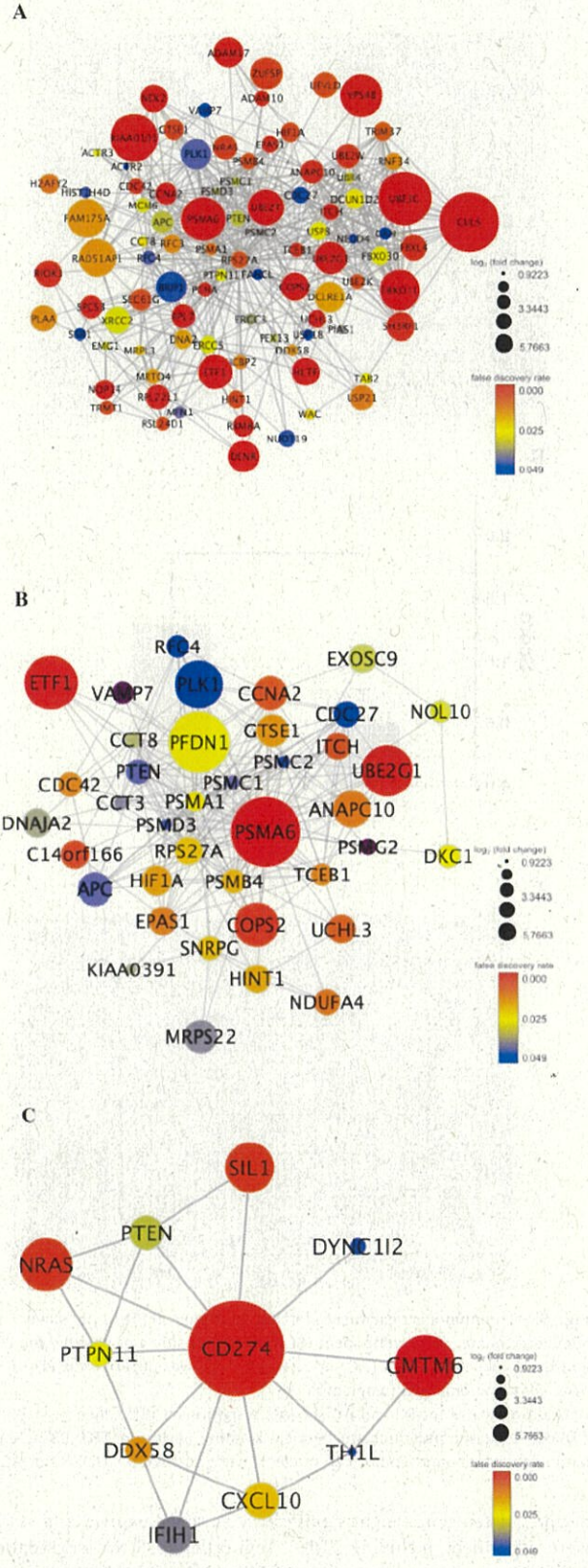

Fig. 4. Protein–protein interaction (PPI) subnetworks.
A) PPI subnetwork of *RPS27A*, a hub gene.
B) PPI subnetwork of *PSMA6*.
C) Subnetwork of *CD274* also known as programmed death ligand-1 (PD-L1).

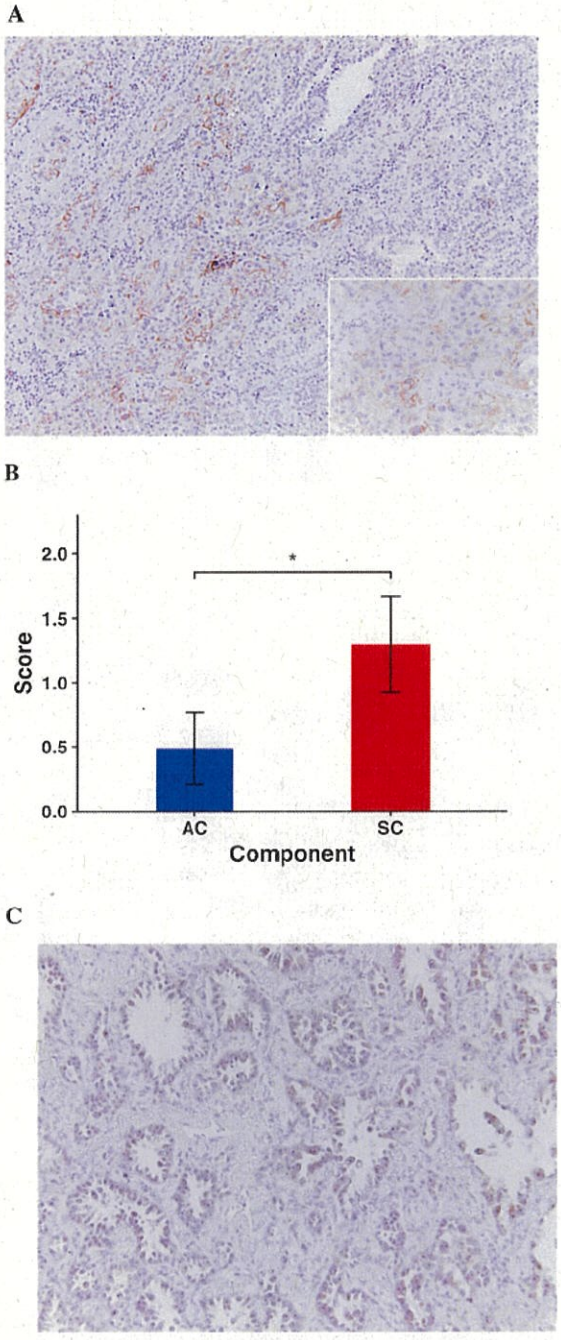

Fig. 5. A) Immunohistochemical staining patterns of PD-L1 in stage I lung adenocarcinoma. Solid component (SC) on the left side was positive for PD-L1 and the acinar component (AC) on the right side was negative for PD-L1. The inset shows an enlarged image of SC.
B) Staining scores for SC and AC showed a significant difference ($p = 0.001$).
C) Representative immunohistochemical staining pattern of HOXB3 in stage I lung adenocarcinoma. Tumor cell nucleoli were positive for HOXB3 in AC.

of upregulated genes, eight significantly enriched pathways ($p < 0.05$) were identified, including "DNA replication," "RNA degradation," "Ubiquitin mediated proteolysis," "Mismatch repair," "Proteasome," "RNA transport," "Cell cycle," and "Terpenoid backbone biosynthesis" (Fig. 3). Most of the pathways were related to cell proliferation, similar to the enriched GO terms. In a network analysis, 658 proteins (nodes) and 3517 interactions (edges) were included. The network was very complicated; however, ribosomal protein S27a (*RPS27a*) was identified as a hub gene with the highest degree (Fig. 4A). *RPS27a* had 94 first neighbors in this network, including *PSMA6* (Fig. 4B). The subnetwork of CD274, known as programmed death ligand 1 (PD-L1), had first neighbors, including CKLF-like MARVEL transmembrane domain-containing 6 (CMTM6) (Fig. 4C).

3.3. Immunohistochemical staining

Representative staining patterns for PD-L1 expression are shown in Fig. 5A. Among 41 cases, 25 cases (61.0 %) showed positive immunostaining for PD-L1 in SC, while 12 cases (29.3 %) were positive in AC (Table 1). The PD-L1-positive status differed significantly between SC and AC ($p = 0.01$). The staining score for PD-L1 was significantly higher in SC than in AC ($p = 0.001$, Fig. 5B). Representative staining patterns for TAF7 expression are shown in Supplementary Fig. 4A. The staining score for TAF7 was tended to be higher in SC than in AC (Supplementary Fig. 4B). Representative staining patterns for HOXB3 expression are shown in Fig. 5C. Among 41 cases, 10 cases (24.4 %) showed positive immunostaining for HOXB3 in SC, while 26 cases (63.4 %) in AC (Table 1). HOXB3-positive status differed significantly between SC and AC ($p = 0.007$).

4. Discussion

SPA is considered an independent predictor of early recurrence or progression-free survival in patients with stage I LUAD [4,22]. The presence of solid pattern even as a minor component in stage I LUADs predicts significantly worse prognosis compared to those without solid pattern. [8]. The characteristic biological mechanisms underlying SPA have been described, *e.g.*, an invasive immunophenotype including increased laminin-5 expression, aggressive tumor microenvironment with higher immune evasion potential, and abundant stromal cells with tumor-promoting function [23,24]. Recently, several studies have reported the molecular profiles of SPA or SC in LUAD using tissue samples [14,15] or databases [16,17]. Zabeck et al. identified inositol-1,4,5-trisphosphate kinase A (*ITPKA*) as an upregulated gene in SC and angiogenin in the lepidic component (LC) [15]. Luo et al. reported that DEGs between SPA and non-SPA are mainly involved in the regulation of water and fluid transport [16]. Dong et al. reported that the expression of PD-L1 is increased in SPA [17]. One study to date has compared the molecular profiles between SPA and acinar predominant adenocarcinoma (APA) in stage I LUAD, showing that SPA is associated with an enrichment in genes involved in RNA polymerase activity as well as the inactivation of the p53 pathway [14]. Because APA is the most frequent subtype in stage I LUAD [3,4], we performed the first analysis of DEGs between SC and AC within the same tumor tissue. We speculated that our approach may contribute to clarify the biological and molecular features associated with the malignant potential of SC. Although further evaluations are required to validate the TAF7 expression in a large number of patients with LUAD, we identified *TAF7* as the most highly upregulated gene in SC. TAF7 acts as a checkpoint regulator in the transition from preinitiation complex (PIC) assembly to transcription initiation [25]. Hao et al. reported that miR-374c-5p suppresses breast cancer development *via* the TAF7-mediated transcriptional regulation of DEP domain-containing 1 (DEPDC1), which is an oncogene in several human cancers, including lung cancer, and is required for biological processes of tumors, including cell proliferation, apoptosis, and metastasis [26]. *TAF7* is reportedly associated with the maintenance of intracellular polyamine levels and the sensitivity to methylglyoxal bis(guanylhydrazone) (MGBG), a polyamine analogue, that induces apoptosis [27]. Furthermore, polyamine-dependent fluorescence probe was developed for selective detection of cancer cells [28]. Our findings and these reports suggest that intracellular polyamine levels may be higher in SC than in AC and serve as a therapeutic target for LUAD with SC. We identified *HOXB3* as the most highly downregulated gene in SC. HOXB3 is a transcription factor that act as a

Table 1
The correlation between histological subtype and PD-L1 or HOXB3 status.

PD-L1	Solid component, n (%)		*p* value	HOXB3	Solid component, n (%)		*p* value
	Positive	Negative			Positive	Negative	
Acinar component, n (%)				Acinar component, n (%)			
Positive	11 (26.8 %)	1 (2.4 %)	0.01	Positive	10 (24.4 %)	16 (39.0 %)	0.007
Negative	14 (34.1 %)	15 (36.6 %)		Negative	0 (0 %)	15 (36.6 %)	

PD-L1; programmed death ligand 1, HOXB3; Homeobox B3.

metastasis suppressor and participates in cell apoptosis, proliferation, migration, invasion, and epithelial-to-mesenchymal transition [29]. In lung adenocarcinoma, epigenetic silencing of HOXB3 was reportedly increased in the metastasizing tumor [30]. Our findings and these reports suggest that epigenetic regulation may be involved in the formation of malignant components, including SC, in LUAD. Additionally, we found that HOXB3 protein was localized in the nucleoli of LUAD cells. Several transcription factors and three homeobox proteins that belong to the Hox family similar to HOXB3, namely HOXB7, HOXC6, and HOXD4, were reported to exhibit the nucleolar localization [31–34]. It has been revealed that nucleoli not only acts as a base of ribosome production, which is main role of nucleoli, but also as a hub of both negative and positive regulation of the tumor development [35], suggesting that nucleolar distribution of HOXB3 may associated with the control of nucleolus-dependent regulation in the LUAD development. Further studies on *in vitro* and *in vivo* are required because there are no therapeutic agents directly targeting either TAF7 or HOXB3; however, they can be considered new therapeutic candidates for LUAD with SC. We also observed that genes annotated with the specific GO terms associated with cell proliferation were upregulated in SC compared to AC. These observations suggest that molecular features based on DEGs analysis reflect the pathological morphology of SC. Additionally, the PPI network of upregulated genes in SC revealed that *RPS27a* as one of hub gene with highest degree. RPS27a is a direct transcriptional target of p53 and is overexpressed in response to DNA damage and in renal, breast, and colon carcinomas [36]. Of the 94 first neighbors in the RPS27a network, we focused on *PSMA6*, a subunit of the proteasome complex, because it is highly expressed in lung cancer cells and is a promising target for lung cancer treatment [37]. *PSMA6* has an oncogenic role in several types of cancer [37]. In turn, Shimoji et al. reported that PD-L1 is expressed in 65 % of SPA but only 16 % of non-SPA cases [38]. We provide the first evidence that the staining score of PD-L1 is higher in SC than in AC within the same tumor tissue. In addition, we focused on the subnetwork of CD274 (PD-L1), which had 10 first neighbor genes, including *CMTM6*, which encodes a ubiquitously expressed protein that binds to PD-L1 and maintains its cell surface expression [39]. It enhances the ability of PD-L1-expressing tumor cells to inhibit T cells [40]. Therefore, we plan to investigate the correlation between PD-L1 and CMTM6 expression in LUAD with SC. Our study has several limitations. Gene expression analysis using NGS includes the small sample size. Another limitation to this study is that the specificity of DEGs for SC was not verified by comparison with other component including lepidic, papillary, and micropapillary. Therefore, further investigations are required to solve these points and identify the therapeutic targets for improving the prognosis of LUAD with SC patients.

5. Conclusions

We showed that *TAF7* is highly upregulated and *HOXB3* is highly downregulated in SC compared to AC within the same tumor tissue. In addition, we identified *PSMA6*, a key gene in lung cancer, as an upregulated first neighbor in the RPS27a network, which is a direct transcriptional target of p53. We also revealed that PD-L1 expression is more common in SC than in AC within the same LUAD tissues. Although further experiments are needed to validate our findings and to clarify the molecular mechanisms underlying the aggressiveness of SC, our results pave the way for contributing to understanding the biological properties leading to the unfavorable prognosis and developing the therapeutic approaches for improving the prognosis in LUAD with SC patients.

Source of funding

This work was supported by JSPS KAKENHI GRANT Number JP19K18214 and JP19K07414.

Declaration of Competing Interest

The authors declare no conflicts of interest.

Acknowledgements

The authors are grateful to Professor Eiji Nanba, Kaori Adachi and Masachika Kai for excellent technical assistance with the processing of the NGS data and to Shoji Yashima and Yuko Urakami for help with the processing of the pathological specimens. This research was partly performed at the Tottori Bio Frontier managed by Tottori prefecture.

Appendix A. Supplementary data

Supplementary material related to this article can be found, in the online version, at doi:https://doi.org/10.1016/j.lungcan.2020.06.035.

References

[1] W.D. Travis, E. Brambilla, A.P. Bruke, A. Marx, A.G. Nicholson, WHO Classification of Tumors of the Lung, Pleura, Thymus, and Heart, 4th ed., Lyon, IARC Press, France, 2015, pp. 26–30.
[2] P. Goldstraw, K. Chansky, J. Crowley, et al., The IASLC lung cancer staging project: proposals for revision of the TNM stage groupings in the forthcoming (eighth) edition of the TNM classification for lung cancer, J. Thorac. Oncol. 11 (2016) 39–51, https://doi.org/10.1016/j.jtho.2015.09.009.
[3] A. Yoshizawa, N. Motoi, G.J. Riely, et al., Impact of proposed IASLC/ATS/ERS classification of lung adenocarcinoma: prognostic subgroups and implications for further revision of staging based on analysis of 514 stage I cases, Mod. Pathol. 24 (2011) 653–664, https://doi.org/10.1038/modpathol.2010.232.
[4] H. Ujiie, K. Kadota, J.E. Chaft, et al., Solid predominant histologic subtype in resected stage I lung adenocarcinoma is an independent predictor of early, extrathoracic, multisite recurrence and of poor postrecurrence survival, J. Clin. Oncol. 26 (2015) 2877–2884, https://doi.org/10.1200/JCO.2015.60.9818.
[5] J.J. Hung, W.J. Jeng, T.Y. Chou, et al., Prognostic value of the new international association for the study of lung Cancer/American thoracic Society/European respiratory society lung adenocarcinoma classification on death and recurrence in completely resected stage I lung adenocarcinoma, Ann. Surg. 258 (2013) 1079–1086, https://doi.org/10.1097/SLA.0b013e31828920c0.
[6] S. Murakami, H. Ito, N. Tsubokawa, et al., Prognostic value of the new IASLC/ATS/ERS classification of clinical stage IA lung adenocarcinoma, Lung Cancer. 90 (2015) 199–204, https://doi.org/10.1016/j.lungcan.2015.06.022.
[7] Y. Kubouchi, Y. Yurugi, M. Wakahara, et al., Podoplanin expression in cancer-associated fibroblasts predicts unfavourable prognosis in patients with pathological stage IA lung adenocarcinoma, Histopathol. 72 (2018) 490–499, https://doi.org/10.1111/his.13390.
[8] T. Chen, J. Luo, H. Gu, et al., Impact of solid minor histologic subtype in postsurgical prognosis of stage I lung adenocarcinoma, Ann. Thorac. Surg. 105 (2018) 302–308, https://doi.org/10.1016/j.athoracsur.2017.08.018.
[9] Y. Mastuoka, Y. Yurugi, Y. Takagi, et al., Prognostic significance of solid and

micropapillary components in invasive lung adenocarcinomas measuring ≤3 cm, Anticancer Res. 36 (2016) 4923–4930, https://doi.org/10.21873/anticanres.11058.
[10] Y. Zhao, R. Wang, X. Shen, et al., Minor components of micropapillary and solid subtypes in lung adenocarcinoma are predictors of lymph node metastasis and poor prognosis, Ann. Surg. Oncol. 23 (2016) 2099–2105, https://doi.org/10.1245/s10434-015-5043-9.
[11] N. Rekhtman, D.C. Ang, G.J. Riely, et al., KRAS mutations are associated with solid growth pattern and tumor-infiltrating leukocytes in lung adenocarcinoma, Mod. Pathol. 26 (2013) 1307–1319, https://doi.org/10.1038/modpathol.2013.74.
[12] H. Hu, Y. Pan, Y. Li, et al., Oncogenic mutations are associated with histological subtypes but do not have an independent prognostic value in lung adenocarcinoma, Onco. Ther. 7 (2014) 1423–1437, https://doi.org/10.2147/OTT.S58900.
[13] C. Molina-Romero, C. Rangel-Escareno, A. Otega-Gomez, et al., Differential gene expression profiles according to the Association for the Study of Lung Cancer/American Thoracic Society/European Respiratory Society histopathological classification in lung adenocarcinoma subtypes, Hum. Pathol. 66 (2017) 188–199, https://doi.org/10.1016/j.humpath.2017.06.002.
[14] J. Zhan, J. Shao, L. Zhu, et al., Molecular profiling identifies prognostic markers of stage IA lung adenocarcinoma, Oncotarget 43 (2017) 74846–74855, https://doi.org/10.18632/oncotarget.20420.
[15] H. Zabeck, H. Dienemann, H. Hoffmann, et al., Molecular signatures in IASLC/ATS/ERS classified growth patterns of lung adenocarcinoma, PLoS One 10 (2018), https://doi.org/10.1371/journal.pone.0206132 e0206132.
[16] J. Luo, K. Ma, Y. Shi, et al., Genetic analyses of differences between solid and nonsolid predominant lung adenocarcinomas, Thor. Cancer 9 (2018) 1656–1663, https://doi.org/10.1111/1759-7714.12876.
[17] Z.Y. Dong, C. Zang, Y.F. Li, et al., Genetic and immune profiles of solid predominant lung adenocarcinoma reveal potential immunotherapeutic strategies, J. Thorac. Oncol. 13 (2017) 85–96, https://doi.org/10.1016/j.jtho.2017.10.020.
[18] R. Hrdlickova, M. Toloue, B. Tian, RNA-Seq methods for transcriptome analysis, Wiley Interdiscip, Rev. RNA. 8 (2017) 1002, https://doi.org/10.1002/wrna.1364.
[19] F. Supek, M. Bosnjak, N. Skunca, T. Smuc, REVIGO summarizes and visualized long lists of gene ontology terms, PLoS One 7 (2011) e21800, , https://doi.org/10.1371/journal.pone.0021800.
[20] D. Szklarczyk, A. Franceschini, S. Wyder, et al., STRING v10: protein-protein interaction networks, integrated over the tree of life, Nucleic Acids Res. 43 (2015) 447–452, https://doi.org/10.1093/nar/gku1003.
[21] P. Shannon, A. Markiel, O. Ozier, et al., Cytoscape: a software environment for integrated models of biomolecular interaction networks, Genome Res. 13 (2003) 2498–2504, https://doi.org/10.1101/gr.1239303.
[22] S. Xu, J. Xi, W. Jiang, S. Lu, Q. Wang, Solid component and tumor size correlate with prognosis of stage IB lung adenocarcinoma, Ann. Thorac. Surg. 99 (2015) 961–967, https://doi.org/10.1016/j.athoracsur.2014.10.079.
[23] K. Saruwatari, S. Ikemura, K. Sekihara, et al., Aggressive tumor microenvironment of solid predominant adenocarcinoma subtype harboring with epidermal growth factor receptor mutations, Lung Cancer. 91 (2016) 7–14, https://doi.org/10.1016/j.lungcan.2015.11.012.
[24] T. Takuwa, G. Ishi, K. Nagai, et al., Characteristic immunophenotype of solid component in lung adenocarcinoma, Ann. Surg. Oncol. 19 (2012) 3943–3952, https://doi.org/10.1245/s10434-012-2428-x.
[25] A. Gegonne, J.D. Weissman, M. Zhou, J.N. Brady, D.S. Singer, TAF7: A possible transcription initiation check-point regulator, PNAS. 103 (2006) 602–607, https://doi.org/10.1073/pnas.0510031103.
[26] S. Hao, W. Tian, Y. Chen, L. Wang, Y. Jiang, B. Gao, MicroRNA-374c-5p inhibits the development of breast cancer through TATA-box binding protein associated factor 7-mediated transcriptional regulation of DEP domain containing 1, J. Cell. Biochem. 120 (2019) 15360–15368, https://doi.org/10.1002/jcb.28803.
[27] J. Fukuchi, R.A. Hiipakka, J.M. Kokontis, et al., TATA-binding protein-associated factor 7 regulates polyamine transport activity and polyamine analog-induced apoptosis, J. Biol. Chem. 279 (2004) 29921–29929, https://doi.org/10.1074/jbc.M401078200.
[28] K.K.H. Vong, K. Tsubokura, Y. Nakao, et al., Cancer cell targeting driven by selective polyamine reactivity with glycine propargyl esters, Chem Commun (Camb). 53 (2017) 8403–8406, https://doi.org/10.1039/c7cc01934c.
[29] F.U. Weiss, I.J. Marques, J.M. Woltering, et al., Retinoic acid receptor antagonists inhibit miR-10a expression and block metastatic behavior of pancreatic cancer, Gastroenterology 137 (2009) 2136–2145, https://doi.org/10.1053/j.gastro.2009.08.065.
[30] I. Daugaard, D. Dominguez, T.E. Kjeldsen, et al., Identification and validation of candidate epigenetic biomarkers in lung adenocarcinoma, Sci. Rep. 6 (2016) 35807, https://doi.org/10.1038/srep35807.
[31] H.A. Feister, K. Torrungruang, P. Thunyakitpisal, et al., NP/NMP4 transcription factors have distinct osteoblast nuclear matrix subdomains, J. Cell. Biochem. 79 (2000) 506–517, https://doi.org/10.1002/1097-4644(20001201)79:3%3C506::AID-JCB150%3E3.0.CO;2-A.
[32] D. Pearce, A. Naray-Fejes-Toth, G. Fejes-Toth, Determinants of subnuclear organization of mineralocorticoid receptor characterized through analysis of wild type and mutant receptors, J. Biol. Chem. 277 (2002) 1451–1456, https://doi.org/10.1074/jbc.M105966200.
[33] C.P. Rubbi, J. Milner, Non-activated p53 co-localizes with sites of transcription within both the nucleoplasm and the nucleolus, Oncogene. 19 (2000) 85–96, https://doi.org/10.1038/sj.onc.1203378.
[34] M.T. Corsetti, G. Levi, F. Lancia, et al., Nucleolar localisation of three Hox homeoproteins, J. Cell. Sci. 108 (1995) 187–193.
[35] D. Stepinski, The nucleolus, an ally, and an enemy of cancer cells, Histochem. Cell Biol. 150 (2018) 607–629, https://doi.org/10.1007/s00418-018-1706-5.
[36] N. Nosrati, N.R. Kapoor, V. Kumar, DNA damage stress induces the expression of Ribosomal Protein S27a gene in a p53-dependent manner, Gene. 559 (2015) 44–51, https://doi.org/10.1016/j.gene.2015.01.014.
[37] T. Kakumu, M. Sato, D. Goto, et al., Identification of proteasomal catalytic subunit PSMA6 as a therapeutic target for lung cancer, Cancer Sci. 108 (207) 732-743. https://doi.org/10.1111/cas.13185.
[38] M. Shimoji, S. Simizu, K. Sato, et al., Clinical and pathological features of lung cancer expressing programmed cell death ligand 1 (PD-L1), Lung Cancer. 98 (2016) 69–75, https://doi.org/10.1016/j.lungcan.2016.04.021.
[39] M.L. Burr, C.E. Sparbier, Y.C. Chan, et al., CMTM6 maintains the expression of PD-L1 and regulates anti-tumour immunitiy, Nature. 549 (2017) 101–105, https://doi.org/10.1038/nature23643.
[40] R. Mezzadra, C. Sun, L.T. Jae, et al., Identification of CMTM6 and CMTM4 as PD-L1 protein regulators, Nature. 549 (2017) 106–110, https://doi.org/10.1038/nature23669.